Hindawi
International Journal of Antennas and Propagation
Volume 2023, Article ID 8851758, 11 pages
https://doi.org/10.1155/2023/8851758

*Research Article*

# A Robust Symbol-Level Precoding Method for Multibeam Satellite Systems

**Qi Wang and Wuyang Zhou**

*School of Information Science and Technology, University of Science and Technology of China, Hefei 230027, China*

Correspondence should be addressed to Wuyang Zhou; wyzhou@ustc.edu.cn

Received 11 May 2023; Revised 3 September 2023; Accepted 25 September 2023; Published 10 October 2023

Academic Editor: Rajkishor Kumar



Compared to interference mitigating precoding, interference exploiting symbol-level precoding (SLP) requires less transmit power to guarantee the quality of service in a multibeam satellite system. However, due to the large roundtrip time (RTT), it is impractical to obtain real-time channel state information on the satellite side. The random channel state information (CSI) phase error of outdated CSI could cause serious performance deterioration of SLP. To compensate the CSI phase error, we propose an outdated CSI-based robust SLP (RSLP) method, which optimizes the transmit power under outage probability constraints. The central limit theorem (CLT) and second-order Taylor expansion are used to relax the outage probability constraints into convex ones. In addition, because only outdated CSI-based robust block-level precoding exists, we present two comparative RSLP methods accordingly. Without violating outrage probability constraints, the proposed RSLP method requires much lower transmit power than comparative RSLP and existing robust block-level precoding methods. The complexity of the proposed RSLP method is also lower than that of two comparative RSLP methods.

## 1. Introduction

A multibeam satellite communication system, which has wide coverage, high spectrum efficiency, and low cost of infrastructure in remote areas, is seen as an important extension of a mobile communication system. By enabling spatial multiplexing, wireless resources such as time and frequency can be effectively reused among multiple beams. However, because of a relatively small beam angle, interbeam interference cannot be ignored; thus, interference management is needed. Interference mitigating block-level precoding (BLP) is a widely used interference management technology to suppress downlink interbeam interference which is treated as an adverse effect [1–3]. Recently, interference exploiting symbol-level precoding (SLP) was proposed to further reduce transmit power or improve the equivalent signal-to-noise ratio (SINR), where channel state information (CSI) and data symbols are taken into account to exploit constructive interference [4–7].

Due to severe channel fading such as path loss, the high transmit power efficiency of precoding is very attractive for satellite systems. Nevertheless, round-trip time (RTT) between a satellite and its user terminals is large, and it is unrealistic for the satellite to obtain perfect CSI to perform precoding. Hence, only outdated CSI can be obtained, where the CSI error is usually modelled as a random phase error [8, 9]. To reduce transmit power with only outdated CSI, robust BLP was studied for unicast [10] and multicast [11]. Besides, the CSI phase error model was also used to design a robust BLP matrix for an integrated satellite-terrestrial system [12] and over line-of-sight channels in a mobile communication system [13]. Besides robust BLP, existing robust SLP (RSLP) methods mainly focused on CSI with an additive error which is a classical model for mobile communication systems. Worst case-based RSLP under bounded channel errors was proposed for PSK constellations in [6] and for generic constellations in [14]. In [15], a probabilistic constructive interference constrained RSLP method was proposed to tackle stochastic channel uncertainties.

Compared with [15], Lyu et al. further improved the outage probability performance [16]. Machine learning-based RSLP was studied in [17, 18], where a Bayesian neural network or a deep neural network was used to design the RSLP vector with much lower execution time. Besides, the MMSE RSLP method under perantenna power constraints was proposed to compensate the CSI error with a more practical model [19]. In [20], the effect of the phase error caused by an oscillator is analyzed, where the phase errors of channels between different beams and specific user are the same. Bounded CSI error-based RSLP is also used for IRS-aided communication systems to reduce transmit power [21]. Although additive error-based RSLP has been studied, further research on outdated CSI-based RSLP enjoys little attention so far.

Consequently, in this paper, we propose a power minimization RSLP method which is under symbol-level outage constraints for the downlink of a multibeam satellite system. The main contributions of the paper are summarized as follows:

(i) We approximate the symbol-level received signals by using both the second-order Taylor expansion and central limit theorem (CLT) to analyze statistical properties. By doing that, the received signal can be seen as a normal distributed variable or a quadratic form of a normal Gaussian distribution vector.

(ii) To solve the symbol-level outage probability constrained power minimization problem, we relax the nonconvex probability constraints into second-order cone (SOC) constraints to obtain the SLP vector. Modified by existing robust BLP methods, two other relaxation methods of outage probability constraints are also designed. Transmit power, outage probabilities and invalid probabilities of three RSLP methods are compared by computer simulation. Numerical results show that our proposed relaxation method is closer to the probabilistic constraints.

*1.1. Notation.* $\mathscr{R}$ and $\mathscr{C}$ are sets of real and complex numbers, respectively. $\mathbf{I}_N$ is the $N \times N$ identity matrix. A user set is denoted by $\mathscr{K} = \{1, 2, ..., K\}$. $\mathbf{1}_{M\times N}$ is the $M \times N$ all-one matrix, and $\mathbf{0}_{M\times N}$ is the all-zero matrix. $\Pr\{X\}$ is the probability of an event $X$. $\odot$ is the Hadamard product operation. $\mathrm{Re}\{\mathbf{x}\}$ is the real part of a vector $\mathbf{x}$, and $\mathrm{Im}\{\mathbf{x}\}$ is the imaginary part. $E\{\mathbf{x}\}$ is the expectation of a random vector $\mathbf{x}$. $\mathrm{Corr}\{\mathbf{x}\}$ is the covariance of $\mathbf{x}$. $\mathrm{Var}\{v\}$ is the variance of random variable $v$. $\mathscr{N}(\mathbf{a}, \mathbf{b})$ is a real Gaussian distribution with a mean vector $\mathbf{a}$ and a covariance matrix $\mathbf{b}$. For any vector $\mathbf{a} = [a_1, a_2, ..., a_n]^T$, we define $\mathrm{pow}(\mathbf{a}, k) = [a_1^k, a_2^k, ..., a_n^k]^T$.

## 2. Materials and Methods

*2.1. System Model and Problem Formulation.* In this section, the multibeam satellite system model is introduced. Besides, we present a brief explanation of constructive interference (CI) to show the effect of interference. When only outdated CSI is known on the satellite side, stochastic robust CI power minimization (SR-CIPM) problem is formulated to compensate the CSI error.

*2.1.1. System Model.* We consider downlink of a multibeam satellite system with $N$ beams, where full frequency reuse is adopted. One resource block is reused by $K$ users, where $K \leqslant N$. The vector of data symbols for $K$ users is denoted by $\mathbf{s} = [s_1, s_2, ...s_K]$. Each entry of $\mathbf{s}$ is from a normalized PSK constellation with order $M$. The normalized receiving signal at the $k$th user side is denoted by the following equation:

$$y_k = \mathbf{h}_k \mathbf{x} + n_k, \forall k \in \mathscr{K}, \tag{1}$$

where $\mathbf{x} \in \mathscr{C}^{N\times 1}$ is the transmit signal vector on the satellite side and the instant transmit power is defined as $P_t = \|\mathbf{x}\|^2$. $n_k \sim \mathscr{CN}(0, 1)$ is the normalized additive Gaussian noise of the $k$th user. $\mathbf{h}_k$ shown in (2) denotes the corresponding block-fading channel vector from the satellite to the $k$th user [8]. $L_k$ is the normalized scale coefficient, which is modelled as shown in (3), where $c$ is the velocity of light, $f_0$ is the carrier frequency, $d_k$ is the distance between the satellite and the $k$th user, $\kappa$ is the Boltzmann constant, $B$ is the signal bandwidth, and $T$ is the noise temperature at the user terminal side. $\widetilde{\boldsymbol{\rho}}_k = \mathrm{pow}(\rho_k, 0.5) \in \mathscr{R}^{1\times N}$ as well as $\ln(\boldsymbol{\rho}_k) \sim \mathscr{N}(\mu_{r,k}\mathbf{1}_{1\times N}, \sigma_{r,k}^2 \mathbf{I}_N)$ denotes the rain attenuation vector for the $k$th user. $\boldsymbol{\varphi}_k \in \mathscr{R}^{1\times N}$ is the channel phase vector, whose elements are uniformly distributed between 0 and $2\pi$. $\mathbf{g}_k$ is the beam gain factor for $k$th UT, whose $i$th entry is given in (4), where $G_{T,i}$ is the transmitting antenna gain of beam $i$, $G_{r,k}$ is the receiving antenna gain of user $k$, and $J_n(.)$ denotes the $n$th order Bessel function of the first kind. The ratio parameter $u_{i,k}$ is set as $u_{i,k} = 2.07123 \sin(\psi_{i,k})/\sin(\psi^{3\mathrm{dB}})$, where $\psi_{i,k}$ is the off-axis angle between the $k$th user and the center of the $i$th beam and $\psi^{3dB}$ is the 3 dB angle of each beam.

$$h_k = \sqrt{L_k}\, \widetilde{\boldsymbol{\rho}}_k \odot \exp\{j\boldsymbol{\varphi}_k\} \odot \mathbf{g}_k \in \mathscr{C}^{1\times N}, \tag{2}$$

$$L_k = \left(\frac{c}{4\pi f_0 d_k}\right)^2 \frac{1}{\kappa \mathrm{BT}}, \tag{3}$$

$$[\mathbf{g}_k]_i = \sqrt{G_{T,i} G_{r,k} \left(\frac{J_1(u_{i,k})}{2u_{i,k}} + 36\frac{J_3(u_{i,k})}{u_{i,k}^3}\right)}. \tag{4}$$

Considering the significant distance between the satellite and any user, the feedback of downlink CSI is outdated. Therefore, a CSI error arises, and here, we describe the error model. According to (2), CSI $\mathbf{h}_k$ depends on the rain attenuation vector $\widetilde{\boldsymbol{\rho}}_k$, the antenna gain vector $\mathbf{g}_k$, the free space path-loss factor $L_k$, and the channel phase vector $\boldsymbol{\varphi}_k$, where $\widetilde{\boldsymbol{\rho}}_k$, $\mathbf{g}_k$, and $L_k$ determine the amplitude of $\mathbf{h}_k$ and $\boldsymbol{\varphi}_k$ determines the phase. It is noteworthy that $L_k$ and $\widetilde{\boldsymbol{\rho}}_k$ are large-scale fading parameters which change relatively slowly. Furthermore, in a short period of time, $\mathbf{g}_k$ can also be regarded constant

since the variation of the off-axis angle between any user and the satellite is very slight. Thus, the amplitude of outdated CSI is approximately equal to that of real CSI. However, due to tropospheric fading, $\boldsymbol{\varphi}_k$ varies when the feedback of CSI is outdated [8–11]. As a result, the large RTT-based CSI error is mainly a phase error. Referring to the widely used random phase error model, we define $\mathbf{h}_k = \mathbf{h}_{\text{est},k} \odot \mathbf{e}_k$, where $\mathbf{h}_{\text{est},k}$ is the known outdated CSI and $\mathbf{e}_k = e^{j\boldsymbol{\theta}_{e,k}^T}$ is the CSI error vector with $\boldsymbol{\theta}_{e,k} \sim \mathcal{N}(\mathbf{0}_{N\times 1}, \boldsymbol{\Sigma}_{e,k})$. $\sum_{e,k} \in \mathscr{R}^{N\times N}$ is assumed perfectly known in this paper, and SINR is used as the quality of service (QoS) metric, where the SINR threshold of the $k$th user is denoted by $\Gamma_k$.

*2.1.2. CI and SR-CIPM Problem Formulation.* The effect of interbeam interference on a specific data symbol is not necessarily adverse. Taking a PSK symbol as an example, if the value of an interference has the similar phase as the symbol, it is more possible for the receiver to correctly demodulate receiving signals. In this case, the interference is constructive and should not be mitigated. The definition of nonstrict CI was proposed in [4] as the interference that pushes the combination of the received signals away from the detection boundary of the known symbol. Based on the definition of CI, the CI region (CIR) was designed as the union of possible signals whose left interference is constructive. To illustrate this, we take a QPSK symbol as an example (as seen in Figure 1). The shadow area in Figure 1 depicts the CI region of a QPSK symbol $s = \sqrt{0.5} + j\sqrt{0.5}$. $A = \sqrt{\Gamma}\sigma \times s$ is the scaled data point, $\Gamma$ is the scaling factor based on SINR threshold, and $\sigma^2$ is the variance of noise. Refer to [5], let $\overrightarrow{\text{OB}} = \lambda s$ where $\lambda$ is a complex multiplier, and point B is in the CI region if

$$(\text{Re}(\lambda) - |\overrightarrow{\text{OA}}|)\tan(\theta) \geq |\text{Im}(\lambda)|, \tag{5}$$

where $\theta = \pi/M$ and $M$ is the modulation order.

The definition of CI tells that whether an interference is constructive is relative with the value of the data symbol. Thus, to ensure that only CI exists, symbol-level signal processing is needed. Because SINR threshold $\Gamma_k$ of the $k$th user is an expectation concept of data symbols, to satisfy the expectation SINR constraints, the nonstrict constructive interference power minimization (CIPM) problem is proposed by constrained instant SINR of the $k$th user not lower than $\Gamma_k$, which is expressed as follows:

$$\begin{aligned} P_1: \quad & \min_{\mathbf{x},\lambda_k} \|\mathbf{x}\|_2^2, \\ \text{s.t.} \quad & C_1: \mathbf{h}_k\mathbf{x} = \lambda_k s_k, \forall k \in \mathscr{K}, \\ & C_2: \left(\text{Re}(\lambda_k) - \sqrt{\Gamma_k}\right)\tan(\phi_k) \geq \left|\text{Im}(\lambda_k)\right|, \forall k \in \mathscr{K}, \end{aligned} \tag{6}$$

where $\lambda_k$ is the scale and rotation factor of $s_k$, $\phi_k = \pi/M$. $C_1$ and $C_2$ ensure that the left interference is constructive. $P_1$ is a linear constrained quadratic programming (LCQP) problem, which can be effectively solved. By denoting

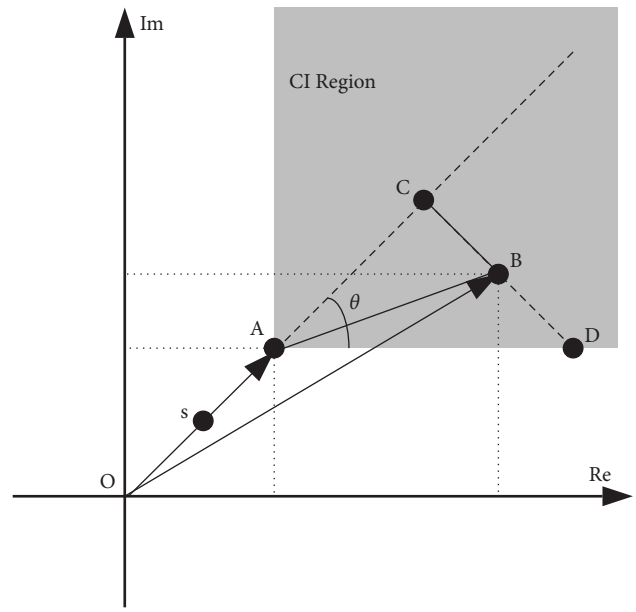


Figure 1: CI region.

$\mathbf{A} = [\mathbf{I}_N, \mathbf{0}_{N\times N}; \mathbf{0}_{N\times N}, -\mathbf{I}_N]$, $\mathbf{B} = [\mathbf{0}_{N\times N}, \mathbf{I}_N; \mathbf{I}_N, \mathbf{0}_{N\times N}]$, $\tilde{\mathbf{x}} = [\text{Re}\{\mathbf{x}^T\}, \text{Im}\{\mathbf{x}^T\}]^T$, and $\tilde{\mathbf{h}}_k = [\text{Re}\{\mathbf{h}_k/s_k\}, \text{Im}\{\mathbf{h}_k/s_k\}] = [\mathbf{r}_{h,k}^T, \mathbf{I}_{h,k}^T]$, we have

$$\begin{aligned} \tilde{\mathbf{h}}_k\mathbf{A}\tilde{\mathbf{x}} &= \text{Re}\left\{\frac{\mathbf{h}_k\mathbf{x}}{s_k}\right\} \\ &= \text{Re}\{\lambda_k\}, \\ \tilde{\mathbf{h}}_k\mathbf{B}\tilde{\mathbf{x}} &= \text{Im}\left\{\frac{\mathbf{h}_k\mathbf{x}}{s_k}\right\} \\ &= \text{Im}\{\lambda_k\}. \end{aligned} \tag{7}$$

Hence, complex optimization problem $P_1$ is equivalent to the real one $P_2$ as shown in the following equation:

$$\begin{aligned} P_2: \quad & \min_{\tilde{\mathbf{x}}} \|\tilde{\mathbf{x}}\|^2, \\ \text{s.t.} \quad & \left|\tilde{\mathbf{h}}_k\mathbf{B}\tilde{\mathbf{x}}\right| \leqslant \tan\phi_k\left(\tilde{\mathbf{h}}_k\mathbf{A}\tilde{\mathbf{x}} - \sqrt{\Gamma_k}\right), \forall k \in \mathscr{K}. \end{aligned} \tag{8}$$

The optimal transmit vector $\mathbf{x}_{\text{opt}}$ of $P_1$ is feasible only when perfect CSI is known. However, perfect CSI is impractical for a satellite to obtain. As shown in Figure 2, because only imperfect CSI $\mathbf{h}_{\text{est},k}$ is known, although $\mathbf{h}_{\text{est},k}\mathbf{x}_{\text{opt}}$ is located in CIR, the real received signal $\mathbf{h}_k\mathbf{x}_{\text{opt}}$ may not satisfy the CI constraint. Therefore, a robust SLP method is needed, and SR-CIPM proposed in [16] is more suitable for a satellite system, which is expressed as follows:

$$\begin{aligned} P_3: \quad & \min_{\tilde{\mathbf{x}}} \|\tilde{\mathbf{x}}\|^2, \\ \text{s.t.} \quad & \Pr\left\{\frac{\left|\tilde{\mathbf{h}}_k\mathbf{B}\tilde{\mathbf{x}}\right|}{\tan\phi_k} \leqslant \tilde{\mathbf{h}}_k\mathbf{A}\tilde{\mathbf{x}} - \sqrt{\Gamma_k}\right\} \geqslant 1 - \eta_k, \forall k \in \mathscr{K}, \end{aligned} \tag{9}$$

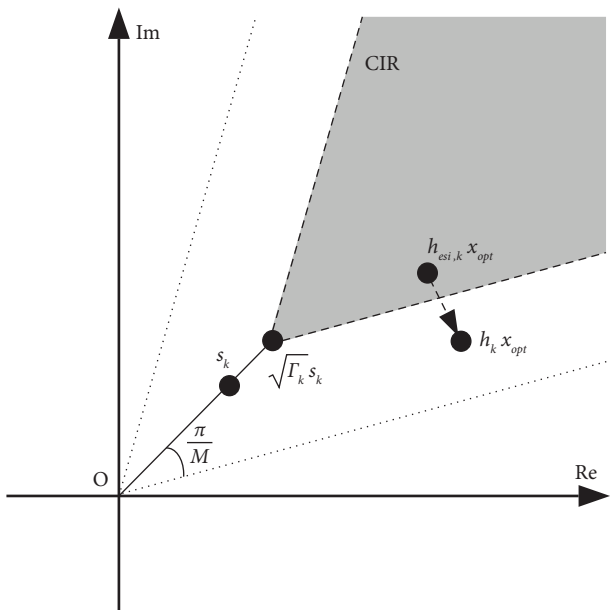


Figure 2: The effect of imperfect CSI.

where $\eta_k$ is defined as a symbol-level robust outage probability hyperparameter. The probability constraint for the $k$th user of $P_3$ is equivalent with

$$\Pr\left\{\tilde{\mathbf{h}}_k \mathbf{C}\tilde{\mathbf{x}} \geq \sqrt{\Gamma_k}, \tilde{\mathbf{h}}_k \mathbf{D}\tilde{\mathbf{x}} \geq \sqrt{\Gamma_k}\right\} \geq 1 - \eta_k, \tag{10}$$

where $\mathbf{C} = (\mathbf{A} - \mathbf{B}/\tan\phi_k)$ and matrix $\mathbf{D} = (\mathbf{A} + \mathbf{B}/\tan\phi_k)$. By defining $\mathscr{A}_k(\tilde{\mathbf{x}}) = \left\{\tilde{\mathbf{h}}_k \,|\, \tilde{\mathbf{x}}^T \mathbf{C}\tilde{\mathbf{h}}_k^T \geq \sqrt{\Gamma_k}\right\}$ and $\mathscr{B}_k(\tilde{\mathbf{x}}) = \left\{\tilde{\mathbf{h}}_k \,|\, \tilde{\mathbf{x}}^T \mathbf{D}\tilde{\mathbf{h}}_k^T \geq \sqrt{\Gamma_k}\right\}$, $P_3$ can be transformed into $P_4$, which is shown in the following equation:

$$\begin{aligned} P_4: \quad & \min_{\tilde{\mathbf{x}}} \|\tilde{\mathbf{x}}\|^2, \\ \text{s.t.} \quad & \Pr\left\{\tilde{\mathbf{h}}_k \in \mathscr{A}_k(\tilde{\mathbf{x}}), \tilde{\mathbf{h}}_k \in \mathscr{B}_k(\tilde{\mathbf{x}})\right\} \geq 1 - \eta_k, \forall k \in \mathscr{K}. \end{aligned} \tag{11}$$

Since the constraints of $P_4$ are nonconvex probability constraints which are difficult to solve, in Section 3, we will solve $P_4$ by approximating the probability constraints into convex ones. The difference between this paper and [16] lies in the model of imperfect CSI, where in [16], the additive error of CSI is assumed, whereas the phase error is supposed in this paper.

*2.2. Robust SLP Methods.* In this section, by approximating $P_4$ into a convex problem, we propose a robust SLP method with outdated CSI. Since previous researchers seldom studied RSLP under imperfect CSI with a phase error, we also propose two comparative RSLP methods accordingly. Besides, the complexity comparison among three RSLP methods is also presented to show that our proposed RSLP method requires the lowest computational complexity.

*2.2.1. Proposed RSLP Method.* Since the probabilistic constraints of $P_4$ are not convex, it is necessary to transform the probabilistic constraints into convex constraints by approximation processing. Due to the fact that $\tilde{\mathbf{x}}^T \mathbf{C}\tilde{\mathbf{h}}_k^T$ and $\tilde{\mathbf{x}}^T \mathbf{D}\tilde{\mathbf{h}}_k^T$ are correlated, the joint probability is difficult to analyze. To simplify the analysis, we refer to the lower bound of joint probability shown in (12) to relax probability constraints [22]. We find that (13) is the sufficient condition of (12), so $P_4$ can be relaxed into $P_5$ in (14). Since the distribution of $\tilde{\mathbf{x}}^T \mathbf{C}\tilde{\mathbf{h}}_k^T$ and $\tilde{\mathbf{x}}^T \mathbf{D}\tilde{\mathbf{h}}_k^T$ is similar to each other, here we only analyze $\Pr\left\{\tilde{\mathbf{h}}_k \notin \mathscr{A}_k(\tilde{\mathbf{x}})\right\}$, whereas $\Pr\left\{\tilde{\mathbf{h}}_k \notin \mathscr{B}_k(\tilde{\mathbf{x}})\right\}$ follows the same steps:

$$\begin{aligned} & \Pr\left\{\tilde{\mathbf{h}}_k \in \mathscr{A}_k(\tilde{\mathbf{x}}), \tilde{\mathbf{h}}_k \in \mathscr{B}_k(\tilde{\mathbf{x}})\right\} \\ & \geq 1 - \Pr\left\{\tilde{\mathbf{h}}_k \notin \mathscr{A}_k(\tilde{\mathbf{x}})\right\} - \Pr\left\{\tilde{\mathbf{h}}_k \notin \mathscr{B}_k(\tilde{\mathbf{x}})\right\} \geq 1 - \eta_k \\ & \Leftrightarrow \Pr\left\{\tilde{\mathbf{h}}_k \notin \mathscr{A}_k(\tilde{\mathbf{x}})\right\} + \Pr\left\{\tilde{\mathbf{h}}_k \notin \mathscr{B}_k(\tilde{\mathbf{x}})\right\} \leq \eta_k, \end{aligned} \tag{12}$$

$$(10) \xrightarrow{\text{relax}} \begin{cases} \Pr\left\{\tilde{\mathbf{h}}_k \notin \mathscr{A}_k(\tilde{\mathbf{x}})\right\} \leq \dfrac{\eta_k}{2}, \\ \Pr\left\{\tilde{\mathbf{h}}_k \notin \mathscr{B}_k(\tilde{\mathbf{x}})\right\} \leq \dfrac{\eta_k}{2}. \end{cases} \tag{13}$$

$$\begin{aligned} P_5: \quad & \min_{\tilde{\mathbf{x}}} \|\tilde{\mathbf{x}}\|^2, \\ \text{s.t.} \quad & (11), \forall k \in \mathscr{K}. \end{aligned} \tag{14}$$

As $\tilde{\mathbf{x}}^T \mathbf{C}\tilde{\mathbf{h}}_k^T$ is the linear combination of multiple random variables, CLT could be used to approximately analyze the distribution of $\tilde{\mathbf{x}}^T \mathbf{C}\tilde{\mathbf{h}}_k^T$ (as a normal variable) [10]. Accordingly, $\tilde{\mathbf{x}}^T \mathbf{C}\tilde{\mathbf{h}}_k^T$ can be approximately described by $E\left\{\tilde{\mathbf{x}}^T \mathbf{C}\tilde{\mathbf{h}}_k^T\right\}$ and $\mathrm{Var}\left\{\tilde{\mathbf{x}}^T \mathbf{C}\tilde{\mathbf{h}}_k^T\right\}$. When $\tilde{\mathbf{x}}$ is fixed, both $E\left\{\tilde{\mathbf{x}}^T \mathbf{C}\tilde{\mathbf{h}}_k^T\right\}$ and $\mathrm{Var}\left\{\tilde{\mathbf{x}}^T \mathbf{C}\tilde{\mathbf{h}}_k^T\right\}$ are functions of the random vector $\mathbf{h}_k$. The relationship between $\mathbf{h}_k$ and $\boldsymbol{\theta}_{e,k}$ is shown as follows:

$$\begin{aligned} \tilde{\mathbf{h}}_k^T &= \begin{bmatrix} \mathbf{r}_{\tilde{h},k} \\ \mathbf{I}_{\tilde{h},k} \end{bmatrix} \\ &= \begin{bmatrix} \mathbf{r}_{\hat{h},k} \odot \cos\left(\boldsymbol{\theta}_{e,k}\right) - \mathbf{I}_{\hat{h},k} \odot \sin\left(\boldsymbol{\theta}_{e,k}\right) \\ \mathbf{r}_{\hat{h},k} \odot \sin\left(\boldsymbol{\theta}_{e,k}\right) + \mathbf{I}_{\hat{h},k} \odot \cos\left(\boldsymbol{\theta}_{e,k}\right) \end{bmatrix}, \end{aligned} \tag{15}$$

where both $\mathbf{r}_{\hat{h},k} = \mathrm{Re}\left\{\mathbf{h}_{\mathrm{est},k}^T / s_k\right\}$ and $\mathbf{I}_{\hat{h},k} = \mathrm{Im}\left\{\mathbf{h}_{\mathrm{est},k}^T / s_k\right\}$ are known on the satellite side. Furthermore, it is easy to obtain $E(\cos\boldsymbol{\theta}_{e,k}) = \tilde{\mathbf{U}}_k \mathbf{1}_{N\times 1}$ and $E(\sin\boldsymbol{\theta}_{e,k}) = \mathbf{0}_{N\times 1}$, where $\tilde{\mathbf{U}}_k = \mathrm{diag}(e^{-\mathbf{u}_k/2})$ and $\mathbf{u}_k$ is the vector of diagonal elements of $\boldsymbol{\Sigma}_{e,k}$. Hence, the mathematical expectation of $\tilde{\mathbf{x}}^T \mathbf{C}\tilde{\mathbf{h}}_k^T$ can be obtained as follows:

$$E\left\{\tilde{\mathbf{x}}^T\mathbf{C}\tilde{\mathbf{h}}_k^T\right\} = \tilde{\mathbf{x}}^T\mathbf{C}\mathbf{U}_k\hat{\mathbf{h}}_k^T, \tag{16}$$

where $\mathbf{U}_k = \begin{bmatrix} \tilde{\mathbf{U}}_k & \mathbf{0}_{N\times N} \\ \mathbf{0}_{N\times N} & \tilde{\mathbf{U}}_k \end{bmatrix}$, $\hat{\mathbf{h}}_k = \left[\mathbf{r}_{\hat{h},k}^T, \mathbf{I}_{\hat{h},k}^T\right]$. Then, by defining $\mathbf{E}_k$ as shown in (17), $\mathrm{Var}\left\{\tilde{\mathbf{x}}^T\mathbf{C}\tilde{\mathbf{h}}_k^T\right\}$ can be derived as shown in (18):

$$\begin{aligned}\mathbf{E}_k &= E\left\{\tilde{\mathbf{h}}_k^T\tilde{\mathbf{h}}_k\right\} \\ &= \begin{bmatrix} \mathbf{E}_{k,1} & \mathbf{E}_{k,2} \\ \mathbf{E}_{k,3} & \mathbf{E}_{k,4} \end{bmatrix} \\ &= \begin{bmatrix} E\left\{\mathbf{r}_{\tilde{h},k}\mathbf{r}_{\tilde{h},k}^T\right\} & E\left\{\mathbf{r}_{\tilde{h},k}\mathbf{I}_{\tilde{h},k}^T\right\} \\ E\left\{\mathbf{I}_{\tilde{h},k}\mathbf{r}_{\tilde{h},k}^T\right\} & E\left\{\mathbf{I}_{\tilde{h},k}\mathbf{I}_{\tilde{h},k}^T\right\} \end{bmatrix},\end{aligned} \tag{17}$$

$$\mathrm{Var}\left\{\tilde{\mathbf{x}}^T\mathbf{C}\tilde{\mathbf{h}}_k^T\right\} = \tilde{\mathbf{x}}^T\mathbf{C}\left(\mathbf{E}_k - \mathbf{U}_k\hat{\mathbf{h}}_k^T\hat{\mathbf{h}}_k\mathbf{U}_k\right)\mathbf{C}^T\tilde{\mathbf{x}}. \tag{18}$$

To calculate the value of $\mathbf{E}_k$, we need to calculate $E\left\{\cos(\boldsymbol{\theta}_{e,k})\cos(\theta_{e,k}^T)\right\}$, $E\left\{\cos(\boldsymbol{\theta}_{e,k})\sin(\boldsymbol{\theta}_{e,k}^T)\right\}$, $E\left\{\sin(\boldsymbol{\theta}_{e,k})\cos(\boldsymbol{\theta}_{e,k}^T)\right\}$, and $E\left\{\sin(\boldsymbol{\theta}_{e,k})\sin(\boldsymbol{\theta}_{e,k}^T)\right\}$, which are difficult to be directly calculated due to the nonindependent property of random vector $\boldsymbol{\theta}_{e,k}$. Therefore, when each element of $\boldsymbol{\theta}_{e,k}$ is relatively small, second-order Taylor expansion can be used. Some intermediate calculation equations are shown in (19), where $\mathbf{t} = [t_1, t_2]^T \sim \mathcal{N}(\mathbf{0}_{2\times1}, \boldsymbol{\Sigma}_\mathbf{t})$ and $\boldsymbol{\Sigma}_\mathbf{t} = \begin{bmatrix} \sigma_{t_1}^2 & \sigma_{t_1}\sigma_{t_2} \\ \sigma_{t_1}\sigma_{t_2} & \sigma_{t_2}^2 \end{bmatrix}$. In (19), it is worth mentioning that only $E\{\cos(t_1)\cos(t_2)\}$ and $E\{\sin(t_1)\sin(t_2)\}$ are approximated by Taylor expansion. When $\sigma_{t_1}^2$ and $\sigma_{t_2}^2$ are relatively small, $E\{t_1^2t_2^2\}$ can be ignored because it is infinitesimal of higher order of $\sigma_{t_1}^2$ and $\sigma_{t_2}^2$.

Thereby, each submatrix of $\mathbf{E}_k$ can be obtained as shown in (20). By defining the symmetric matrix $\tilde{\mathbf{E}}_k = (\mathbf{E}_k - \mathbf{U}_k\hat{\mathbf{h}}_k^T\hat{\mathbf{h}}_k\mathbf{U}_k)$, there exists an orthogonal matrix $\mathbf{Q}_k \in \mathscr{R}^{2N\times2N}$, diagonal matrix $\boldsymbol{\Lambda}_k \in \mathscr{R}^{2N\times2N}$, and matrix $\mathbf{F} \in \mathscr{R}^{2N\times2N}$ so that $\tilde{\mathbf{E}}_k = \mathbf{F}\mathbf{F}^T = \mathbf{Q}_k^T\boldsymbol{\Lambda}_k^{1/2}\boldsymbol{\Lambda}_k^{1/2}\mathbf{Q}_k$. Thus, $\mathrm{Var}\left\{\tilde{\mathbf{x}}^T\mathbf{C}\tilde{\mathbf{h}}_k^T\right\} = \|\mathbf{F}^T\mathbf{C}^T\tilde{\mathbf{x}}\|_2^2$ can be obtained:

$$\begin{aligned}E\left\{\cos^2(t_1)\right\} &= \frac{1}{2}\left(1 + e^{-2\sigma_{t_1}^2}\right), \\ E\left\{\sin^2(t_1)\right\} &= \frac{1}{2}\left(1 - e^{-2\sigma_{t_1}^2}\right), \\ E\{\cos(t_1)\sin(t_1)\} &= 0, \\ E\{\cos(t_1)\cos(t_2)\} &\approx 1 - \frac{1}{2}\sigma_{t_1}^2 - \frac{1}{2}\sigma_{t_2}^2 + \frac{1}{4}E\left\{t_1^2t_2^2\right\}, \\ E\left\{t_1^2t_2^2\right\} &= 3\sigma_{t_1}^4\sigma_{t_1t_2}^4 + 2\sigma_{t_1t_2}^8 + 4\sigma_{t_1}^2\sigma_{t_1t_2}^4\sigma_{t_2}^2 + 3\sigma_{t_1t_2}^4\sigma_{t_2}^4, \\ E\{\sin(t_1)\sin(t_2)\} &\approx \sigma_{t_1}^2, \\ E\{\sin(t_1)\cos(t_2)\} &= E\{\cos(t_1)\sin(t_2)\} = 0,\end{aligned} \tag{19}$$

$$\begin{aligned}\mathbf{E}_{k,1}(i,j) &\approx \begin{cases} \frac{1}{2}\mathbf{r}_{\hat{h},k}^2(i)\left(1 + e^{-2\boldsymbol{\Sigma}_{e,k}(i,i)}\right) + \frac{1}{2}\mathbf{I}_{\hat{h},k}^2(i)\left(1 - e^{-2\boldsymbol{\Sigma}_{e,k}(i,i)}\right), \text{if } i = j, \\ \left(1 - \frac{1}{2}\boldsymbol{\Sigma}_{e,k}(i,i) - \frac{1}{2}\boldsymbol{\Sigma}_{e,k}(j,j)\right)\mathbf{r}_{\hat{h},k}(i)\mathbf{r}_{\hat{h},k}(j) + \boldsymbol{\Sigma}_{e,k}(i,j)\mathbf{I}_{\hat{h},k}(i)\mathbf{I}_{\hat{h},k}(j), \text{if } i \neq j, \end{cases} \\ \mathbf{E}_{k,2}(i,j) &\approx \begin{cases} e^{-2\boldsymbol{\Sigma}_{e,k}(i,i)}\mathbf{r}_{\hat{h},k}(i)\mathbf{I}_{\hat{h},k}(i), , \text{if } i = j, \\ \left(1 - \frac{1}{2}\boldsymbol{\Sigma}_{e,k}(i,i) - \frac{1}{2}\boldsymbol{\Sigma}_{e,k}(j,j)\right)\mathbf{r}_{\hat{h},k}(i)\mathbf{I}_{\hat{h},k}(j) - \boldsymbol{\Sigma}_{e,k}(i,j)\mathbf{I}_{\hat{h},k}(i)\mathbf{r}_{\hat{h},k}(j), \text{if } i \neq j, \end{cases} \\ \mathbf{E}_{k,3}(i,j) &\approx \begin{cases} e^{-2\boldsymbol{\Sigma}_{e,k}(i,i)}\mathbf{I}_{\hat{h},k}(i)\mathbf{r}_{\hat{h},k}(i), \text{if } i = j, \\ \left(1 - \frac{1}{2}\boldsymbol{\Sigma}_{e,k}(i,i) - \frac{1}{2}\boldsymbol{\Sigma}_{e,k}(j,j)\right)\mathbf{I}_{\hat{h},k}(i)\mathbf{r}_{\hat{h},k}(j) - \boldsymbol{\Sigma}_{e,k}(i,j)\mathbf{r}_{\hat{h},k}(i)\mathbf{I}_{\hat{h},k}(j), \text{if } i \neq j, \end{cases} \\ \mathbf{E}_{k,4}(i,j) &\approx \begin{cases} \frac{1}{2}\mathbf{I}_{\hat{h},k}^2(i)\left(1 + e^{-2\boldsymbol{\Sigma}_{e,k}(i,i)}\right) + \frac{1}{2}\mathbf{r}_{\hat{h},k}^2(i)\left(1 - e^{-2\boldsymbol{\Sigma}_{e,k}(i,i)}\right), \text{if } i = j, \\ \left(1 - \frac{1}{2}\boldsymbol{\Sigma}_{e,k}(i,i) - \frac{1}{2}\boldsymbol{\Sigma}_{e,k}(j,j)\right)\mathbf{I}_{\hat{h},k}(i)\mathbf{I}_{\hat{h},k}(j) + \boldsymbol{\Sigma}_{e,k}(i,j)\mathbf{r}_{\hat{h},k}(i)\mathbf{r}_{\hat{h},k}(j), \text{if } i \neq j. \end{cases}\end{aligned} \tag{20}$$

After the approximation of the mean and variance of $\tilde{\mathbf{x}}^T\mathbf{C}\tilde{\mathbf{h}}_k^T$ and $\tilde{\mathbf{x}}^T\mathbf{D}\tilde{\mathbf{h}}_k^T$ has been derived, the marginal probability $\Pr\{\tilde{\mathbf{h}}_k \notin \mathscr{A}_k(\tilde{\mathbf{x}})\}$ and $\Pr\{\tilde{\mathbf{h}}_k \notin \mathscr{B}_k(\tilde{\mathbf{x}})\}$ can be approximated as follows:

$$\Pr\{\tilde{\mathbf{h}}_k \notin \mathscr{A}_k(\tilde{\mathbf{x}})\} \approx \frac{1}{2}\left(1 - \operatorname{erf}\left(\frac{\tilde{\mathbf{x}}^T\mathbf{C}\mathbf{U}_k\hat{\mathbf{h}}_k^T - \sqrt{\Gamma_k}}{\sqrt{2}\left\|\mathbf{F}^T\mathbf{C}^T\tilde{\mathbf{x}}\right\|}\right)\right),$$

$$\Pr\{\tilde{\mathbf{h}}_k \notin \mathscr{B}_k(\tilde{\mathbf{x}})\} \approx \frac{1}{2}\left(1 - \operatorname{erf}\left(\frac{\tilde{\mathbf{x}}^T\mathbf{D}\mathbf{U}_k\hat{\mathbf{h}}_k^T - \sqrt{\Gamma_k}}{\sqrt{2}\left\|\mathbf{F}^T\mathbf{D}^T\tilde{\mathbf{x}}\right\|}\right)\right). \tag{21}$$

Referring to [16], we could therefore transform the probability optimization problem $P_5$ into an SOC problem (SOCP) $P_6$ as shown in (22), where $a_0 = \operatorname{erf}^{-1}(1-\eta_k)$, $\operatorname{erf}^{-1}(.)$ is the inverse error function. SOCP $P_6$ is convex and can be effectively solved using the CVX toolbox:

$$\begin{aligned} P_6: \quad & \min_{\tilde{\mathbf{x}}} \|\tilde{\mathbf{x}}\|^2 \\ \text{s.t.} \quad & C_1: \sqrt{2}a_0\left\|\mathbf{F}^T\mathbf{C}^T\tilde{\mathbf{x}}\right\| \leqslant \hat{\mathbf{h}}_k\mathbf{U}_k\mathbf{C}\tilde{\mathbf{x}} - \sqrt{\Gamma_k}, \forall k \in \mathscr{K}, \\ & C_2: \sqrt{2}a_0\left\|\mathbf{F}^T\mathbf{D}^T\tilde{\mathbf{x}}\right\| \leqslant \hat{\mathbf{h}}_k\mathbf{U}_k\mathbf{D}\tilde{\mathbf{x}} - \sqrt{\Gamma_k}, \forall k \in \mathscr{K}. \end{aligned} \tag{22}$$

*2.2.2. Comparison RSLP Methods.* Because the solution of the proposed RSLP methods is not optimal for $P_5$, a benchmark is needed for performance comparison. However, previous researchers seldom studied RSLP under imperfect CSI with a phase error. Therefore, referring to robust BLP, we present two comparative RSLP methods.

Referring to [10], if an outage condition can be formulated as a quadratic inequality of a CSI phase error, the outage probability constraint can be relaxed into a convex one. Therefore, in following paragraphs, by employing two different convex approximation methods, $P_5$ can be transformed into two separate convex problems, both of which can be effectively solved.

We directly use the second-order Taylor expansion to approximate $\tilde{\mathbf{h}}_k$ [9], which is shown in the following equation:

$$\tilde{\mathbf{h}}_k^T \approx \begin{bmatrix} \operatorname{Re}\left\{\hat{\mathbf{h}}_k^T\right\} \odot \left(1 - \dfrac{\boldsymbol{\theta}_{e,k}^2}{2}\right) - \operatorname{Im}\left\{\hat{\mathbf{h}}_k^T\right\} \odot \boldsymbol{\theta}_{e,k} \\ \operatorname{Re}\left\{\hat{\mathbf{h}}_k^T\right\} \odot \boldsymbol{\theta}_{e,k} + \operatorname{Im}\left\{\hat{\mathbf{h}}_k^T\right\} \odot \left(1 - \dfrac{\boldsymbol{\theta}_{e,k}^2}{2}\right) \end{bmatrix}. \tag{23}$$

Meanwhile, by defining $\tilde{\boldsymbol{\theta}}_{e,k} = \sum_{e,k}^{-1/2}\boldsymbol{\theta}_{e,k} \sim \mathscr{N}(\mathbf{0}_{N\times 1}, \mathbf{I}_N)$, $\tilde{\mathbf{x}}_{\mathbf{C}} = \mathbf{C}\tilde{\mathbf{x}} = [\tilde{\mathbf{x}}_{C,1}^T, \tilde{\mathbf{x}}_{C,2}^T]^T$ and intermediate parameters $\boldsymbol{\Lambda}_{k,1}^{(C)}$, $\boldsymbol{\Lambda}_{k,2}^{(C)}$, $\mathbf{L}_k^{(C)}(\tilde{\mathbf{x}})$, and $\mathbf{f}_k^{(C)}(\tilde{\mathbf{x}})$ shown in (24) and (25) can be derived. Similarly, $\boldsymbol{\Lambda}_{k,1}^{(D)}$, $\boldsymbol{\Lambda}_{k,2}^{(D)}$, $\mathbf{L}_k^{(D)}(\tilde{\mathbf{x}})$, $\mathbf{f}_k^{(D)}(\tilde{\mathbf{x}})$, and $\tilde{\mathbf{h}}_k\tilde{\mathbf{x}}_{\mathbf{D}}$ can be obtained by defining $\tilde{\mathbf{x}}_{\mathbf{D}} = \mathbf{D}\tilde{\mathbf{x}} = [\tilde{\mathbf{x}}_{D,1}^T, \tilde{\mathbf{x}}_{D,2}^T]^T$:

$$\begin{aligned} \boldsymbol{\Lambda}_{k,1}^{(C)} &= \mathbf{r}_{\hat{h},k} \odot \tilde{\mathbf{x}}_{C,1} + \mathbf{I}_{\hat{h},k} \odot \tilde{\mathbf{x}}_{C,2}, \\ \boldsymbol{\Lambda}_{k,2}^{(C)} &= \mathbf{r}_{\hat{h},k} \odot \tilde{\mathbf{x}}_{C,2} - \mathbf{I}_{\hat{h},k} \odot \tilde{\mathbf{x}}_{C,1}, \\ \mathbf{L}_k^{(C)}(\tilde{\mathbf{x}}) &= -\frac{1}{2}\boldsymbol{\Sigma}_{e,k}^{1/2}\operatorname{diag}\left(\boldsymbol{\Lambda}_{k,1}^{(C)}\right)\boldsymbol{\Sigma}_{e,k}^{1/2}, \\ \mathbf{f}_k^{(C)}(\tilde{\mathbf{x}}) &= \boldsymbol{\Sigma}_{e,k}^{1/2}\boldsymbol{\Lambda}_{k,2}^{(C)}, \end{aligned} \tag{24}$$

$$\tilde{\mathbf{h}}_k\tilde{\mathbf{x}}_{\mathbf{C}} \approx \tilde{\boldsymbol{\theta}}_{e,k}^T\mathbf{L}_k^{(C)}(\tilde{\mathbf{x}})\tilde{\boldsymbol{\theta}}_{e,k} + \mathbf{f}_k^{(C)}(\tilde{\mathbf{x}})\tilde{\boldsymbol{\theta}}_{e,k} + \mathbf{1}^T\boldsymbol{\Lambda}_{k,1}^{(C)}. \tag{25}$$

In (25), with given $\tilde{\mathbf{x}}$, the approximation of $\tilde{\mathbf{h}}_k\tilde{\mathbf{x}}_{\mathbf{C}}$ is a quadratic function of a standard normal random vector, and so is $\tilde{\mathbf{h}}_k\tilde{\mathbf{x}}_{\mathbf{D}}$. With method III in [23] or Lemma 2 in [13], the probability constraints $\Pr\{\tilde{\mathbf{h}}_k \notin \mathscr{A}_k(\tilde{\mathbf{x}})\}$ and $\Pr\{\tilde{\mathbf{h}}_k \notin \mathscr{B}_k(\tilde{\mathbf{x}})\}$ can be transformed into convex constraints (25) or (26), respectively. $a_{k,C}$, $a_{k,D}$, $b_{k,C}$, and $b_{k,D}$ are new optimization parameters, and $v_k \geqslant \sqrt{2}$ is the solution of $(1/2 - 1/(v_k^2))v_k = \sqrt{\ln(1/(1-\eta_k))}$. In this way, $P_5$ can be transformed into the SOCP problem $P_7$ shown in (28) or a semidefinite program (SDP) problem $P_8$ shown in (29), where $\mathbf{a}_{\mathbf{C}} = [a_{1,C}, a_{2,C}, ..., a_{K,C}]^T$, $\mathbf{b}_{\mathbf{C}} = [b_{1,C}, b_{2,C}, ..., b_{K,C}]^T$, $\mathbf{a}_{\mathbf{D}} = [a_{1,D}, a_{2,D}, ..., a_{K,D}]^T$, and $\mathbf{b}_{\mathbf{D}} = [b_{1,D}, b_{2,D}, ..., b_{K,D}]^T$:

$$\begin{cases} \mathbf{1}^T\boldsymbol{\Lambda}_{k,1}^{(C)} - \sqrt{\Gamma_k} + \operatorname{Tr}\left\{\mathbf{L}_k^{(C)}(\tilde{\mathbf{x}})\right\} \leqslant 2\sqrt{-\ln(1-\eta_k)}\left(a_{k,C} + b_{k,C}\right), \\ \mathbf{1}^T\boldsymbol{\Lambda}_{k,1}^{(D)} - \sqrt{\Gamma_k} + \operatorname{Tr}\left\{\mathbf{L}_k^{(D)}(\tilde{\mathbf{x}})\right\} \leqslant 2\sqrt{-\ln(1-\eta_k)}\left(a_{k,D} + b_{k,D}\right), \\ \dfrac{1}{\sqrt{2}}\left\|\mathbf{f}_k^{(C)}(\tilde{\mathbf{x}})\right\|_2 \leqslant a_{k,C}, \dfrac{1}{\sqrt{2}}\left\|\mathbf{f}_k^{(D)}(\tilde{\mathbf{x}})\right\|_2 \leqslant a_{k,D}, \\ v_k\left\|\mathbf{L}_k^{(C)}(\tilde{\mathbf{x}})\right\|_F \leqslant b_{k,C}, v_k\left\|\mathbf{L}_k^{(D)}(\tilde{\mathbf{x}})\right\|_F \leqslant b_{k,D}, \end{cases}$$

$$\begin{cases} \mathrm{Tr}\left\{\mathbf{L}_k^{(C)}(\tilde{\mathbf{x}})\right\} + 1^T \boldsymbol{\Lambda}_{k,1}^{(C)} \geqslant 2\sqrt{\ln\dfrac{1}{1-\eta_k}}\, a_{k,C} - 2b_{k,C}\ln(1-\eta_k), \\ \mathrm{Tr}\left\{\mathbf{L}_k^{(D)}(\tilde{\mathbf{x}})\right\} + 1^T \boldsymbol{\Lambda}_{k,1}^{(D)} \geqslant 2\sqrt{\ln\dfrac{1}{1-\eta_k}}\, a_{k,D} - 2b_{k,D}\ln(1-\eta_k), \\ \sqrt{\left\|\mathbf{L}_k^{(C)}(\tilde{\mathbf{x}})\right\|_F^2 + 2\left\|\mathbf{f}_k^{(C)}(\tilde{\mathbf{x}})\right\|} \leqslant a_{k,C}, \sqrt{\left\|\mathbf{L}_k^{(D)}(\tilde{\mathbf{x}})\right\|_F^2 + 2\left\|\mathbf{f}_k^{(D)}(\tilde{\mathbf{x}})\right\|} \leqslant a_{k,C}, \\ b_{k,C}\mathbf{I}_K + \mathbf{L}_k^{(C)}(\tilde{\mathbf{x}}) \succcurlyeq 0, b_{k,D}\mathbf{I}_K + \mathbf{L}_k^{(D)}(\tilde{\mathbf{x}}) \succcurlyeq 0, \end{cases} \tag{27}$$

$$P_7: \quad \min_{\tilde{\mathbf{x}},\mathbf{a}_C,\mathbf{b}_C,\mathbf{a}_D,\mathbf{b}_D} \|\tilde{\mathbf{x}}\|^2, \quad \text{s.t.} \quad (25), \forall k \in \mathcal{K}. \tag{28}$$

$$P_8: \quad \min_{\tilde{\mathbf{x}},\mathbf{a}_C,\mathbf{b}_C,\mathbf{a}_D,\mathbf{b}_D} \|\tilde{\mathbf{x}}\|^2, \quad \text{s.t.} \quad (26), \forall k \in \mathcal{K}. \tag{29}$$

*2.2.3. Complexity Analysis.* The computational complexity of the proposed RSLP method is mainly dominated by computing the orthogonal decomposition of each $\widetilde{\mathbf{E}}_k$ and by solving the SOCP problem $P_6$. $O((2N)^3)$ is usually used as the complexity of orthogonal decomposition of the $2N \times 2N$ matrix $\widetilde{\mathbf{E}}_k$. $K$ matrices are needed to be decomposed per symbol duration; thus, $O(\mathrm{KN}^3)$ is the complexity of orthogonal decomposition. The worst-case complexity analysis is usually used to evaluate computational complexity of solving the SOCP problem by using the interior point method [15, 24], where the complexity of obtaining an $\varepsilon$-solution is shown as follows:

$$C_{\mathrm{SOCP}}(\epsilon) = n(2m+l)^{1/2}\left(n^2 + l(n+1) + \sum_{i=1}^{m} k_i^2\right)O(1)\ln\frac{1}{\epsilon}, \tag{30}$$

where $n$ is the dimension of the optimization vector, $m$ is the number of SOCs, $l$ is the number of linear constraints, $k_i$ is the size of the $i$th second-order cone, and $\epsilon$ is the optimization accuracy variable. The complexity of solving SOCP $P_6$ is shown in (31). Therefore, the total complexity of the proposed RSLP method is $C_{P_6} + O(\mathrm{KN}^3)$:

$$C_{P_6}(\epsilon) = (2N+1)\sqrt{4K+2}\left(2(2N+1)^2 + 8\mathrm{KN}^2\right)\ln\frac{1}{\epsilon}O(1). \tag{31}$$

It is worth noting that if $\boldsymbol{\Sigma}_{e,k} = \sigma_{e,k}^2\mathbf{I}_K$ from [8], four $N \times N$ submatrices of $\widetilde{\mathbf{E}}_k$ are all diagonal matrices. Accordingly, $\widetilde{\mathbf{E}}_k$ can be transformed into a block diagonal matrix by exchanging rows and columns, where each diagonal subblock is a $2 \times 2$ matrix. The complexity of orthogonal decomposition of that block diagonal matrix is $N \times O(2^3)$; thereby, the total complexity can be reduced:

$$C_{P_7} = (2N+4K+1)\sqrt{10K+2}\left((2N+4K+1)^2 + 2K(2N+4K+2) + (4K+1)(2N+1)^2\right)O(1)\ln\frac{1}{\epsilon}, \tag{32}$$

$$C_{\mathrm{SDP}}(\epsilon) = \left(2m + l + \sum_{i=1}^{p} g_i\right)^{1/2} n\left(n^2 + l(n+1) + \sum_{i=1}^{m} k_i^2 + n\sum_{i=1}^{p} g_i^2 + \sum_{i=1}^{p} g_i^3\right)O(1)\ln\frac{1}{\epsilon}, \tag{33}$$

$$C_{P_8}(\varepsilon) = (2KN+6K+2)^{1/2}(2N+4K+1)\left(\begin{array}{c}(2N+4K+1)^2 + 2K(2K+4K+2) + 2\mathrm{KN}^3 + \\ +(2K+1)(2N+1)^2 + (2N+4K+1)2\mathrm{KN}^2\end{array}\right)O(1)\ln\frac{1}{\epsilon}. \tag{34}$$

The complexity of comparative RSLP methods is mainly dominated by solving SOCP $P_7$ or SDP $P_8$, where the complexity bound of $P_7$ is shown in (32). The complexity of $P_8$ is much higher than that of $P_6$ and $P_7$ due to the semidefinite constraints. The complexity of solving an SDP problem is shown in (33), where $g_i$ is the dimension of the $i$th semidefinite constraint and $p$ is the total number of semidefinite constraints [24]. The complexity of $P_8$ is shown in (34). For clarity, when $N \to \infty (N \geqslant K)$, the complexity comparison among three convex problems is shown in Table 1.

Table 1: Complexity comparison.

| | $P_6$ | $P_7$ | $P_8$ |
|---|---|---|---|
| $n$ | $2N+1$ | $2N+4K+1$ | $2N+4K+1$ |
| $l$ | 0 | $2K$ | $2K$ |
| $m$ | $2K+1$ | $4K+1$ | $4K+1$ |
| $k_1$ | $2N$ | $2N+1$ | $2N+1$ |
| $k_i, \forall i \neq 1$ | $2N+1$ | $2N+1$ | $2N+1$ |
| $p$ | 0 | 0 | $2K$ |
| $g_i, \forall i = 1, 2, ..., p$ | 0 | 0 | $N$ |
| $C(N \to \infty, N \geqslant K)$ | $O(K^{3/2}N^3)$ | $O(K^{3/2}N^3)$ | $O(K^{3/2}N^{9/2})$ |

Table 2: Simulation factor.

| Parameters | Value |
|---|---|
| Orbit altitude | 35900 km |
| Carrier frequency ($f_c$) | 20 GHz |
| Boltzmann's constant ($\kappa$) | $1.38 \times 10^{-23}$ Joule/K |
| Bandwidth (B) | 100 MHz |
| Satellite antenna gain | 38 dBi |
| Receiver G/T | 15 dB/K |
| $\psi_{3\text{dB}}$ | $0.4^\circ$ |
| Rain-fading mean | −2.6 dB |
| Rain-fading variance | 1.63 dB |
| $\Gamma_k$ | 7 dB |
| Constellation type | 8 PSK |
| Noise temperature | 298 K |

## 3. Results and Discussion

In this section, numerical results of average transmit power, outage probabilities (OPs), and invalid probabilities of the proposed robust SLP method and two comparative SLP methods are presented and analyzed by using Monte Carlo simulations, where 200 samples of $K = 6$ user location parameters are randomly generated. $L_1 = 5$ blocks are transmitted for one sample, and $L_2 = 20$ time slots are in one block. RSLP is performed on $N = 6$ beams of the satellite. Besides, we assume $\mathbf{\Sigma}_{e,k} = 0.5\sigma_e \mathbf{I}_N + 0.5\sigma_e \mathbf{1}_{N\times N}, \forall k \in \mathcal{K}$, and $\mathbf{e}_k$ and $\mathbf{e}_j$ are independent for $\forall k \neq j$. The maximum instant transmit power for any time slot is set as $\text{PdBW}_{\max}$. Other simulation factors are shown in Table 2.

It is crucial to highlight that the proposed SLP method and two comparative SLP methods are not always feasible. Namely, a feasible solution for $P_6$, $P_7$, or $P_8$ does not always exist. In those three problems, two main factors affecting the existence of a feasible solution are the covariance matrices of the CSI error $\mathbf{\Sigma}_{e,1}, \mathbf{\Sigma}_{e,2}, ..., \mathbf{\Sigma}_{e,K}$ and SINR thresholds $\Gamma_1, \Gamma_2, ..., \Gamma_K$. $\mathbf{\Sigma}_{e,k}$ represents the channel condition, where larger $\sigma_e$ brings about more significant phase uncertainty, making it more challenging for the precoder to guarantee the QoS requirement. $\Gamma_k$ reflects the QoS requirement of the $k$th user, and larger $\Gamma_k$ also increases the difficulty of meeting QoS constraints. Besides, given a maximum instant transmit power limit, if the optimal transmit signal $\mathbf{x}_{\text{opt}}$ obtained from $P_6$, $P_7$, or $P_8$ has a large power ($\|\mathbf{x}_{\text{opt}}\|^2 > P_{\max}$), it is still not a feasible solution. As a result, during simulation, if no feasible solution exists for any time slot, we utilize nonrobust zero-forcing transmit signals with a maximum instant transmit power. Meanwhile, when the power of the optimal transmit signal exceeds $P_{\max}$, we employ the scaled optimal transmit signal $c\mathbf{x}_{\text{opt}}$, ensuring that its power matches $P_{\max}$.

Because there are few RSLP methods under phase error for comparison, we also provide numerical results of block-level outage probability constrained robust block precoding methods with outdated CSI. For clarity, abbreviations used in this section are shown as follows:

(1) "ZF": the nonrobust zero-forcing (ZF) BLP

(2) "CIPM": the nonrobust CI constrained power minimization SLP [6]

(3) "LDI": the large deviation inequality (LDI)-aided robust BLP method [10]

(4) "OCRBP": the outage constrained robust BLP method based on $\mathcal{S}$-procedure [11]

(5) "OSCI-SR-CIPM": the proposed outdated CSI-based SR-CIPM SLP $P_6$

(6) "C-RSLP1": the RSLP method $P_7$ for comparison

(7) "C-RSLP2": the RSLP method $P_8$ for comparison

The average transmit power is defined as follows:

$$P_{\text{ave}} = \frac{\sum_{l_1}^{L_1} \sum_{l_2}^{L_2} P_t(l_1, l_2)}{L_1 L_2}, \tag{35}$$

where $P_t(l_1, l_2) = \|\mathbf{x}(l_1, l_2)\|^2$ is the instant power of the $l_2$ th time slot in the $l_1$ th block. Figure 3 depicts the average transmit power of proposed and comparative RSLP methods with different $\sigma_e$. In Figure 3, the OSCI-SR-CIPM method has better power performance than C-RSLP1 and C-RSLP2. Average transmit power is higher with smaller OP threshold. That is because smaller OP threshold makes CI probability constraints stricter. Although the transmit power of LDI is smaller than that of proposed OSCI-SR-CIPM with small $\sigma_e$, its symbol-level OP performance is not good, which can be seen in Figure 4.

Figure 4 shows the statistical outage probabilities of proposed and comparative precoding methods with different $\sigma_e$. In Figure 4, nonrobust ZF, CIPM, and two robust BLP methods have unacceptable symbol-level OP performance. Besides, although it seems that two comparative methods have better OP performance than that of the proposed RSLP method, it is worth noting that the OSCI-SR-CIPM method satisfies the OP constraints with lower transmit power in most cases, which means that the relaxed constraints of the OSCI-SR-CIPM method match OP constraints better.

From Figure 4, we can also find that with higher $\sigma_e$, the OPs of three RSLP methods are all increased. There are two reasons for that result, one of which is that all the three methods use the Taylor expansion to approximate probability constraints, and with higher $\sigma_e$, the accuracy of the Taylor expansion is deteriorated. Another reason is that with higher $\sigma_e$, invalid probabilities of three methods are higher. Moreover, OPs of C-RSLP1 and C-RSLP2 increase much faster than those of OSCI-SR-CIPM. That is because

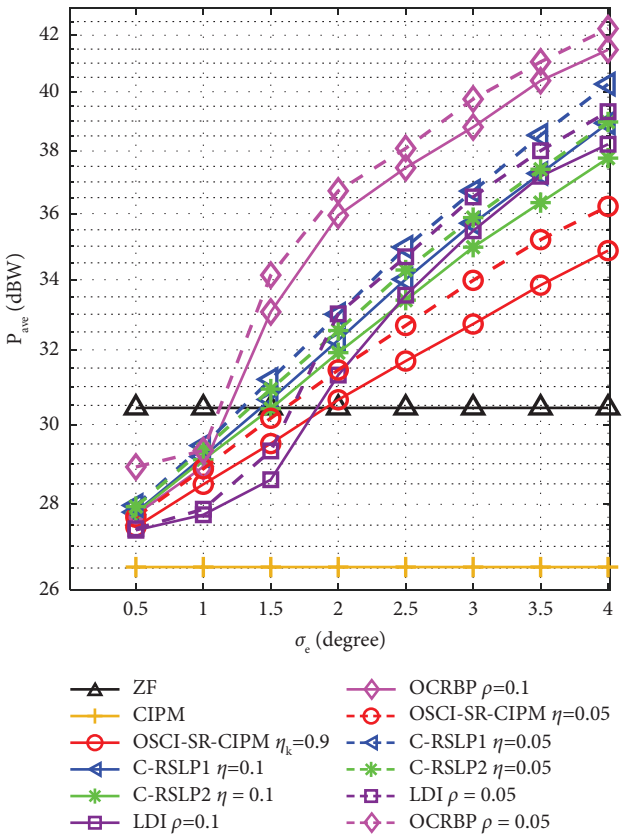


Figure 3: Average transmit power with different $\sigma_e$.

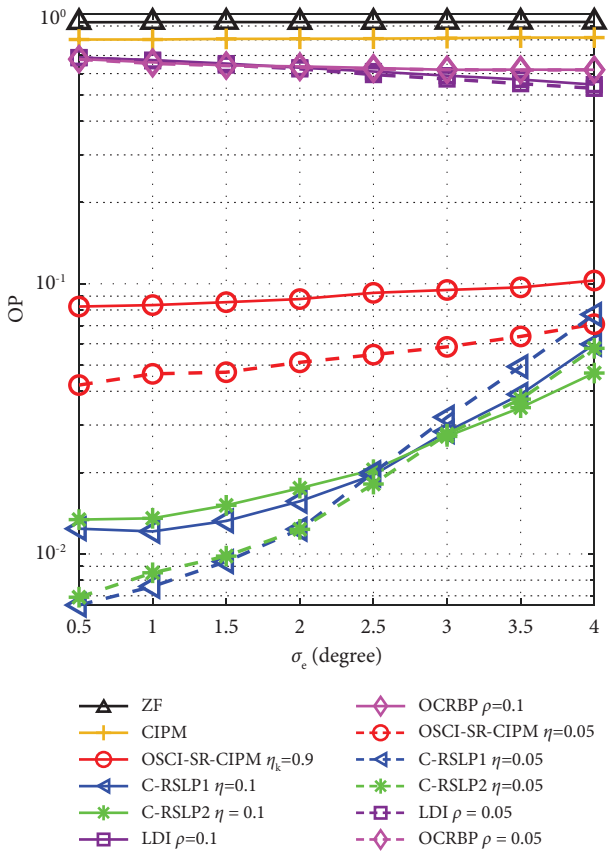


Figure 4: Outage probability with different $\sigma_e$.

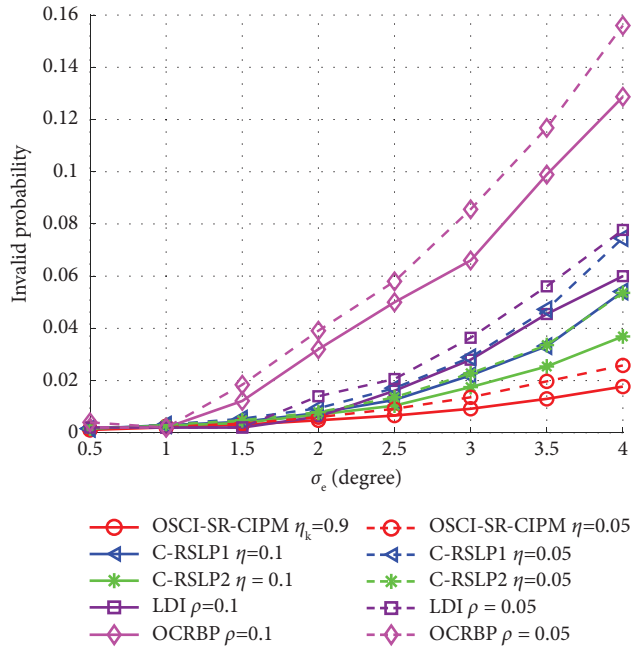


Figure 5: Invalid probability with different $\sigma_e$.

invalid probabilities of two comparative methods increase faster than those of OSCI-SR-CIPM, which is shown in Figure 5. All of the three RSLP methods are designed to solve the same nonconvex problem $P_5$, where the difference lies in the ways to relax nonconvex probability constraints into convex ones. The difference of invalid probability performance in Figure 5 reflects the effect of relaxation of three methods, where the OSCI-SR-CIPM method has better approximation, and the relaxation constraints of C-RSLP1 and C-RSLP2 are stricter. The reason is that to relax probability constraints (12), both C-RSLP1 and C-RSLP2 use the second-order Taylor expansion to approximate $\tilde{\mathbf{h}}_k$. Then, based on that approximation, another relaxation of the probability constraints of $\tilde{\mathbf{x}}^T\mathbf{C}\tilde{\mathbf{h}}_k^T$ and $\tilde{\mathbf{x}}^T\mathbf{D}\tilde{\mathbf{h}}_k^T$ is used; thus, two relaxation steps are needed. OSCI-SR-CIPM directly analyzes the statistical property of $\tilde{\mathbf{x}}^T\mathbf{C}\tilde{\mathbf{h}}_k^T$ and $\tilde{\mathbf{x}}^T\mathbf{D}\tilde{\mathbf{h}}_k^T$, which can be seen as Gaussian distribution variables, and then, we only use the second-order Taylor expansion to approximate a few parts of $\mathbf{E}_k$ to obtain $\mathrm{Var}\left\{\tilde{\mathbf{x}}^T\mathbf{D}\tilde{\mathbf{h}}_k^T\right\}$ and $\mathrm{Var}\left\{\tilde{\mathbf{x}}^T\mathbf{D}\tilde{\mathbf{h}}_k^T\right\}$; thus, fewer relaxation steps are needed.

## 4. Conclusions

In this paper, we solved SR-CIPM for PSK constellations to compensate the phase error of outdated CSI. CLT and second-order Taylor expansion are used to relax the probability constraints into convex ones. Based on different approximation methods, OSCI-SR-CIPM and two comparative RSLP methods are proposed. Simulation results show that although all the three RSLP methods could satisfy the OP constraints with relatively low phase error variance, OSCI-SR-CIPM has the lowest average transmit power and invalid probability.

For future work, because the proposed RSLP method is only feasible for PSK constellations, the RSLP method for other constellations such as QAM is also needed. But it is more difficult to design RSLP over QAM constellations because the CIRs of some QAM constellation points are bounded and very small. Thus, it is impractical to constrain the symbol-level outage probability. Due to the difficulty of directly designing RSLP over QAM constellations, we will use symbol-level signal processing to improve the power efficiency of robust BLP. Moreover, besides outdated CSI, which can be seen as multiplicative noise of channels, imperfect feedback CSI also exists in a practical satellite system. In this case, both addictive and multiplicative errors of a channel should be compensated.

## Data Availability

The dataset of the simulation is available from the corresponding author on reasonable request.

## Conflicts of Interest

The authors declare that there are no conflicts of interest.

## Acknowledgments

This work was supported by the National Key Research and Development Program of China (Grant no. 2018YFB1801105).

## References

[1] L. You, K.-X. Li, J. Wang, X. Gao, X.-G. Xia, and B. Ottersten, "Massive mimo transmission for leo satellite communications," *IEEE Journal on Selected Areas in Communications*, vol. 38, no. 8, pp. 1851–1865, 2020.

[2] C. Qi and X. Wang, "Precoding design for energy efficiency of multibeam satellite communications," *IEEE Communications Letters*, vol. 22, no. 9, pp. 1826–1829, 2018.

[3] K.-X. Li, L. You, J. Wang et al., "Downlink transmit design for massive mimo leo satellite communications," *IEEE Transactions on Communications*, vol. 70, no. 2, pp. 1014–1028, 2022.

[4] M. Alodeh, S. Chatzinotas, and B. Ottersten, "Constructive multiuser interference in symbol level precoding for the miso downlink channel," *IEEE Transactions on Signal Processing*, vol. 63, no. 9, pp. 2239–2252, 2015.

[5] A. Li and C. Masouros, "Interference exploitation precoding made practical: optimal closed-form solutions for psk modulations," *IEEE Transactions on Wireless Communications*, vol. 17, no. 11, pp. 7661–7676, 2018.

[6] C. Masouros and G. Zheng, "Exploiting known interference as green signal power for downlink beamforming optimization," *IEEE Transactions on Signal Processing*, vol. 63, no. 14, pp. 3628–3640, 2015.

[7] A. Li, C. Masouros, B. Vucetic, Y. Li, and A. L. Swindlehurst, "Interference exploitation precoding for multi-level modulations: closed-form solutions," *IEEE Transactions on Communications*, vol. 69, no. 1, pp. 291–308, 2021.

[8] W. Wang, L. Gao, R. Ding et al., "Resource efficiency optimization for robust beamforming in multi-beam satellite communications," *IEEE Transactions on Vehicular Technology*, vol. 70, no. 7, pp. 6958–6968, 2021.

[9] Y. Xiao, D. Mishra, J. Yuan, and Y. Luo, "Proportionally fair robust beamforming for multicast multibeam satellite systems," *IEEE Communications Letters*, vol. 26, no. 1, pp. 128–132, 2022.

[10] X. Zhang, J. Wang, C. Jiang, C. Yan, Y. Ren, and L. Hanzo, "Robust beamforming for multibeam satellite communication in the face of phase perturbations," *IEEE Transactions on Vehicular Technology*, vol. 68, no. 3, pp. 3043–3047, 2019.

[11] Y. Yan, K. An, B. Zhang, S. Li, and D. Guo, "Outage constrained robust beamforming for multicast multibeam satellite systems with a phase error," *IEEE Transactions on Aerospace and Electronic Systems*, vol. 56, no. 5, pp. 4152–4156, 2020.

[12] J. Chu and X. Chen, "Robust design for integrated satellite–terrestrial internet of things," *IEEE Internet of Things Journal*, vol. 8, no. 11, pp. 9072–9083, 2021.

[13] M.-C. Yue, S. X. Wu, and A. M.-C. So, "A robust design for miso physical-layer multicasting over line-of-sight channels," *IEEE Signal Processing Letters*, vol. 23, no. 7, pp. 939–943, 2016.

[14] A. Haqiqatnejad, S. Shahbazpanahi, and B. Ottersten, "A worst-case performance optimization based design approach to robust symbol-level precoding for downlink mu-mimo," in *Proceedings of the 2019 IEEE Global Conference on Signal and Information Processing (GlobalSIP)*, pp. 1–5, IEEE, Ottawa, ON, Canada, November 2019.

[15] A. Haqiqatnejad, F. Kayhan, and B. Ottersten, "Robust sinr-constrained symbol-level multiuser precoding with imperfect channel knowledge," *IEEE Transactions on Signal Processing*, vol. 68, pp. 1837–1852, 2020.

[16] G. Lyu, Y. You, A. Li, X. Liao, and C. Masouros, "Probabilistic constructive interference precoding for imperfect csit," *IEEE Transactions on Vehicular Technology*, vol. 70, no. 4, pp. 3932–3937, 2021.

[17] J. Zhang, C. Masouros, and M. Rodrigues, "Robust symbol-level precoding beyond csi models: a probabilistic-learning based approach," in *Proceedings of the 2021 IEEE Global Communications Conference (GLOBECOM)*, pp. 1–6, Madrid, Spain, December 2021.

[18] A. Mohammad, C. Masouros, and Y. Andreopoulos, "Learning-based symbol level precoding: a memory-efficient unsupervised learning approach," in *Proceedings of the 2022 IEEE Wireless Communications and Networking Conference (WCNC)*, pp. 429–434, IEEE, Austin, TX, USA, April 2022.

[19] E. S. Lopes and L. T. Landau, "Mmse symbol level precoding under a per antenna power constraint for multiuser mimo systems with psk modulation," *IEEE Wireless Communications Letters*, vol. 11, no. 11, pp. 2440–2444, 2022.

[20] L. M. Marrero, A. Haqiqatnejad, J. C. M. Duncan, S. Chatzinotas, and B. Ottersten, "Multiuser-miso precoding under channel phase uncertainty in satellite communication systems," *IEEE Open Journal of Vehicular Technology*, vol. 4, pp. 127–148, 2023.

[21] G. Zhang, C. Shen, B. Ai, and Z. Zhong, "Robust symbol-level precoding and passive beamforming for irs-aided communications," *IEEE Transactions on Wireless Communications*, vol. 21, no. 7, pp. 5486–5499, 2022.

[22] E. S. Lopes, L. T. Landau, and A. Mezghani, "Minimum union bound symbol error probability precoding for psk modulation and phase quantization," in *Proceedings of the 2022 IEEE Globecom Workshops (GC Wkshps)*, pp. 1681–1686, IEEE, Rio de Janeiro, Brazil, December 2022.

[23] K.-Y. Wang, A. M.-C. So, T.-H. Chang, W.-K. Ma, and C.-Y. Chi, "Outage constrained robust transmit optimization for multiuser miso downlinks: tractable approximations by conic optimization," *IEEE Transactions on Signal Processing*, vol. 62, no. 21, pp. 5690–5705, 2014.

[24] A. Ben-Tal and A. Nemirovski, *Lectures on Modern Convex Optimization: Analysis, Algorithms, and Engineering Applications*, SIAM, New delhi, India, 2001.